

A numerically efficient output-only system-identification framework for stochastically forced self-sustained oscillators

Minwoo Lee^a, Kyu Tae Kim^b, Jongho Park^{c,*}

^aDepartment of Mechanical Engineering, Hanbat National University, Daejeon 34158, Korea

^bDepartment of Aerospace Engineering, Korea Advanced Institute of Science and Technology (KAIST), Daejeon 34141, Korea

^cComputer, Electrical and Mathematical Science and Engineering Division, King Abdullah University of Science and Technology (KAUST), Thuwal 23955, Saudi Arabia

Abstract

Self-sustained oscillations are ubiquitous in nature and engineering. In this paper, we propose a novel output-only system-identification framework for identifying the system parameters of a self-sustained oscillator affected by Gaussian white noise. A Langevin model that characterizes the self-sustained oscillator is postulated, and the corresponding Fokker–Planck equation is derived from stochastic averaging. From the drift and diffusion terms of the Fokker–Planck equation, unknown parameters of the system are identified. We develop a numerically efficient algorithm for enhancing the accuracy of parameter identification. In particular, a modified Levenberg–Marquardt optimization algorithm tailored to output-only system identification is introduced. The proposed framework is demonstrated on both numerical and experimental oscillators with varying system parameters that develop into self-sustained oscillations. The results show that the computational cost required for performing the system identification is dramatically reduced by using the proposed framework. Also, system parameters that were difficult to be extracted with the existing method could be efficiently computed with the system identification method developed in this study. Pertaining to the robustness and computational efficiency of the presented framework, this study can contribute to an accurate and fast diagnosis of dynamical systems under stochastic forcing.

Keywords: System identification, Self-sustained oscillation, Derivative-free optimization, Levenberg–Marquardt algorithm, Fokker–Planck equation

2020 MSC: 90C53, 90C56, 90C26, 65Z05

1. Introduction

A self-sustained oscillation, also known as self-excited oscillation or autonomous oscillation, in a nonlinear system occurs from a balance between the driving energy source and the damping mechanism [1, 2]. In a noise-free environment, the amplitude of a self-sustained oscillation does not grow or decay in time, while the dynamics of such an oscillation is governed by the oscillator itself, rather than the initial conditions [3]. Self-sustained oscillation is found ubiquitously in many natural and engineered systems, including heartbeat [4], stellar pulsations [5], hydrodynamic [6, 7], thermoacoustic [8, 9] and aeroacoustic [10] oscillations, to name just a few.

Over the past few decades, much effort has been devoted to understanding and describing the dynamics of self-sustained oscillations. This is because, in practical engineered systems, vibrations characterized by self-sustained oscillation are often detrimental. For instance, self-sustained thermoacoustic oscillations that are induced by positive feedback between pressure and heat release rate oscillation in a combustor can induce vibration and fatigue, decreasing the lifetime of the overall system [11]. It is therefore important to be able to understand the characteristics of self-sustained oscillation, so as to predict, avoid or control such an oscillation.

*Corresponding author

Email addresses: mwlee@hanbat.ac.kr (Minwoo Lee), kt_kim@kaist.ac.kr (Kyu Tae Kim), jongho.park@kaust.edu.sa (Jongho Park)

URL: <https://sites.google.com/view/jonghopark> (Jongho Park)

A promising method for understanding the dynamics of a self-sustained oscillator is the system identification approach, which is a type of inverse problem. In a system identification approach, a low-order model is postulated to describe the system’s dynamics¹, and the parameters of that model are identified [10, 13, 14]. Two classes of the system-identification framework are present—input-output and output-only. In the input-output framework [7, 9, 15, 16, 17], system’s response to the input signal is used for system identification. In this framework, one can adjust the intensity of the forcing (i.e., the input signal), so as to induce the desired response of the system that is optimal for system identification. For example, coherence resonance [18, 19] that occurs at an intermediate intensity of noise input can be artificially induced to perform the system identification [7]. However, it is often difficult or impractical to apply external forcing in many systems. High-pressure oscillations occurring in rocket combustors and gas turbines, for example, are difficult to be perturbed by external forcing owing to the high energy required. In such cases, the output-only framework [20, 21, 22, 23] that relies solely on the output signal of the system should be applied. In this framework, observable data inherent to the system is processed using various tools, such as modal identification [24], autosynchronization [20] and sparse regression [25], for finding the unknown parameters of the system.

A notable approach in output-only system identification of self-sustained oscillators utilizes the effect of random fluctuations acting on the system. Unlike the conventional viewpoint that noise is considered as signal contamination, this approach focuses on the dynamic effect of noise that drives the oscillator away from its original dynamical state. For this purpose, statistical methods based on the Langevin equation and the corresponding Fokker–Planck equation are used to extract the deterministic information from the stochastic signal. This type of output-only system-identification framework has been demonstrated in various systems, both numerically and experimentally [10, 21, 22, 23, 26, 27].

One of the main challenges when applying the above-mentioned system-identification framework is to overcome the adverse *finite-time effect*. This effect is caused by the non-Markovian nature of the noise, owing to the coarse sampling rate or the band-pass filtering around the major oscillation frequency, notwithstanding the Markovian assumption of memoryless noise. An efficient method for addressing the finite-time effect is to use the adjoint Fokker–Planck equation for estimating the deterministic parameters of the system [28, 29]. Specifically, Boujo and Noiray [22] showed that coefficients of Van der Pol-type self-sustained oscillator can be accurately extracted via optimization based on adjoint Fokker–Planck equation. In their study, a direct search method, namely the Nelder–Mead optimization [30, 31], is performed to minimize the difference between experimental and mathematical drift/diffusion terms, identifying the parameters that best represent the dynamics of self-sustained oscillation. In a more recent study, this framework is experimentally validated on an aeroacoustic system [32].

In this study, we build on the previous work by [22], focusing on the numerical efficiency of the system identification. Although the established adjoint-based system identification method provides sufficiently accurate system parameters, it requires much computational cost for optimization. This is because the convergence rate of direct search methods can be very slow [33]; direct search methods do not utilize the first- or higher-order derivatives of the cost function to improve the convergence rate. Considering the practical applications, however, it is important that the system identification is conducted quickly. This is because, in many systems (e.g., gas turbines or rocket combustors), it is often essential to perform instantaneous preventive or circumventive measures for self-sustained oscillation, before such oscillation causes severe system damage.

Addressing this issue, we further develop the adjoint-based output-only system-identification framework by improving its numerical aspect. We first observe that the optimization model used in output-only system identification is a nonlinear least-squares problem. Although Gauss–Newton-type algorithms such as the Levenberg–Marquardt algorithm [34] are known to be good choices to ensure fast convergence for nonlinear least-squares problems [35], we cannot directly apply them to our optimization model because it is difficult to compute the first-order derivatives of the cost function. For the sake of achieving the convergence rate comparable to Gauss–Newton-type methods without the information of the first-order derivatives, we propose a novel optimization algorithm for the output-only system identification. We construct the optimization algorithm by replacing the Jacobian terms in the Levenberg–Marquardt algorithm by their suitable finite difference approximations. Since the proposed algorithm can efficiently utilize an approximated derivative information of the cost function to find a good search direction, we hypothesize that such an algorithm can find an optimum of the system identification model along a more optimized trajectory, compared to

¹System model can sometimes be identified from the system-identification process itself [12].

the conventional Nelder–Mead algorithm. Thus, it is expected that the proposed algorithm requires a much smaller number of residual computations than the Nelder–Mead algorithm, implying that the computational cost of the proposed algorithm can be dramatically improved. From the proposed approach, we aim to lessen the computational cost required for the optimization, enhancing the overall efficiency of the system-identification framework.

This paper is organized as follows. In Section 2, we review the established system-identification framework of stochastically forced self-sustained oscillators and relevant existing numerical algorithms. In Section 3, we propose a new numerical algorithm for solving the optimization model for system identification. Numerical results and gas-turbine combustor experiments that highlight the robustness of the proposed algorithm are presented in Section 4. We conclude the paper with remarks in Section 5.

2. System-identification framework

In this section, we review the system-identification framework for stochastically forced self-sustained oscillators presented in [22, 23]. We first present the Fokker–Planck equation that is derived from the Langevin model characterizing the self-sustained oscillator under random forcing. Then we review the optimization-based output-only system-identification method [22, 23] that enables the extraction of system parameters from the drift and diffusion terms of the Fokker–Planck equation.

2.1. Fokker–Planck equation

We consider a phenomenological model for a self-sustained oscillator under stochastic forcing [2, 36]. Specifically, a Langevin equation characterizing a Van der Pol-type oscillator perturbed by additive white Gaussian noise is postulated:

$$\frac{d^2x}{dt^2} - (\epsilon + \alpha x^2) \frac{dx}{dt} + \omega^2 x = \sqrt{2d}\eta, \quad t > 0, \quad (2.1)$$

where $x(t)$ is the instantaneous state of the system, $\eta(t)$ is a unit white Gaussian noise term, d is the noise amplitude, ω is the angular frequency, ϵ is the linear growth (positive) or decay (negative) coefficient, and α is the negative nonlinear coefficient. Specifically, the system is in the linearly stable regime at $\epsilon < 0$, crosses the Hopf point at $\epsilon = 0$, and develops a self-sustained oscillation in the linearly unstable regime at $\epsilon > 0$. In this paper, we not only consider the self-sustained oscillation at $\epsilon > 0$ but also consider the negative or zero ϵ cases, as the system identification at the latter cases can lead to a prediction of self-sustained oscillations [37].

To find a probabilistic solution of (2.1), we consider the following Fokker–Planck equation, which is obtained by stochastic averaging of (2.1) (see Appendix A):

$$\begin{aligned} \frac{\partial}{\partial t} P(a, t) &= -\frac{\partial}{\partial a} [D^{(1)}(a)P(a, t)] + \frac{\partial^2}{\partial a^2} [D^{(2)}(a)P(a, t)], \quad a > 0, \quad t > 0, \\ P(a, 0) &= P_0(a), \quad a > 0, \\ P(0, t) &= 0, \quad t > 0, \end{aligned} \quad (2.2)$$

where $P(a, t)$ is the transitional probability density function of a at time t , $D^{(1)}(a)$ and $D^{(2)}(a)$ are the Kramer–Moyal coefficients, and $P_0(a)$ is the initial probability density at $t = 0$. Specifically, $D^{(1)}(a)$ and $D^{(2)}(a)$ represent the drift and diffusion terms, respectively, and are given by

$$D^{(1)}(a) = \frac{\epsilon}{2}a + \frac{\alpha}{8}a^3 + \frac{d}{2\omega^2 a}, \quad D^{(2)}(a) = \frac{d}{2\omega^2}. \quad (2.3)$$

2.2. System identification model

Among the unknown parameters of the Langevin equation (2.1), we can easily identify ω from spectral analysis, specifically by inspecting the power spectral density. Although the noise may induce a shift in ω due to the anisochronicity factor [38], for simplicity, we assume that ω is independent of d , as in [9]. Finding other system parameters, namely ϵ , α and d , is a more challenging task. While the most straightforward way to identify these parameters using the observed instantaneous state $x(t)$ is the extrapolation method, which is described in Appendix B, it

is known to be prone to the adverse effect of the finite-time effect. Here, we summarize key features of the optimization model for system identification proposed in [22, 23], which alleviates the adverse finite-time effect.

The starting point is the Fokker–Planck equation (2.2). In order to extract the system parameters ϵ , α , and d of (2.1), the drift ($D^{(1)}(a)$) and diffusion ($D^{(2)}(a)$) terms in (2.2) have to be first identified. Siegert et al. [39] have shown that, these terms can be computed from the time correlation of the output signal. More precisely, for $n = 1, 2$ and $a > 0$, we have

$$D^{(n)}(a) = \lim_{\tau \rightarrow 0} D_{\tau}^{(n)}(a), \quad (2.4)$$

where $D_{\tau}^{(n)}(a)$ is defined by

$$D_{\tau}^{(n)}(a) = \frac{1}{n! \tau} \int_0^{\infty} (A - a)^n P(A, t + \tau | a, t) dA. \quad (2.5)$$

In (2.5), $P(A, t + \tau | a, t)$ denotes the conditional probability density function of the oscillation amplitude being A at time $t + \tau$ in case where the amplitude is a at time t . Using the identity (2.5), one can obtain the approximate value of $D_{\tau}^{(n)}(a)$ without analytically solving the Fokker–Planck equation (2.2).

Assume that the system state $x(t)$ is available on the time interval $t \in [0, T_{\max}]$ for some $T_{\max} > 0$. We choose a set of time-shifts $\{\tau_j\}_{j=1}^{N_{\tau}}$ on the time interval for some positive integer N_{τ} . Applying the Hilbert transform, amplitude $a(t)$ can be extracted from $x(t)$. We can then choose a set of amplitudes $\{a_i\}_{i=1}^{N_a}$ in the range of $a(t)$ for some positive integer N_a . In the remainder of this section, let the indices i and j run from 1 to N_a and N_{τ} , respectively. Each point (a_i, τ_j) will play a role of a sampling point in the amplitude-time space for system identification. A discrete approximation of the conditional probability density function $P(A, t + \tau | a, t)$ in (2.5) can be computed on the grid consisting of the points (a_i, τ_j) using the amplitude data $a(t)$. Then the integral in (2.5) can be evaluated by a numerical integration scheme such as the simple trapezoidal rule. In what follows, we denote the value of $D_{\tau}^{(n)}(a)$ at $a = a_i$ and $\tau = \tau_j$ computed from the system state $x(t)$ by the above-mentioned procedure as $\widehat{D}_{\tau_j}^{(n)}(a_i)$. That is, $\widehat{D}_{\tau_j}^{(n)}(a_i)$ depends on $x(t)$ only, so that a priori knowledge on the parameters ϵ , α , and d in (2.1) is not required in the computation of $\widehat{D}_{\tau_j}^{(n)}(a_i)$.

In the optimization model proposed in [22, 23], we minimize the ℓ^2 -difference between the experimental data $\widehat{D}_{\tau_j}^{(n)}(a_i)$ and the coefficient-based data $D_{\tau_j}^{(n)}(a_i)$. Here, the latter value should be calculated from a solution of the Fokker–Planck equation (2.2). However, it is generally difficult to obtain a solution to the standard Fokker–Planck equation (2.2), either analytically or numerically [40]. Therefore, we alternatively consider the following *adjoint* Fokker–Planck equation with the system coefficients ϵ , α and d [22, 28]:

$$\begin{aligned} \frac{\partial}{\partial t} P^{\dagger}(A, t) &= D^{(1)}(A) \frac{\partial}{\partial A} P^{\dagger}(A, t) + D^{(2)}(A) \frac{\partial^2}{\partial A^2} P^{\dagger}(A, t), \quad A > 0, t > 0, \\ P^{\dagger}(A, 0) &= (A - a)^n, \quad A > 0, \\ P^{\dagger}(0, t) &= 0, \quad t > 0, \end{aligned} \quad (2.6)$$

where $D^{(1)}(A)$ and $D^{(2)}(A)$ are given in (2.3). We solve (2.6) numerically, yielding an approximate $D_{\tau_j}^{(n)}(a_i)$ value [28]:

$$D_{\tau_j}^{(n)}(a_i) = \frac{P^{\dagger}(a_i, \tau_j)}{n! \tau}. \quad (2.7)$$

Now, we consider the following cost function that measures an weighted ℓ^2 -error between $\widehat{D}_{\tau_j}^{(n)}(a_i)$ and $D_{\tau_j}^{(n)}(a_i)$ when the parameters ϵ , α , and d in (2.1) vary:

$$E(\epsilon, \alpha, d) = \frac{1}{2N_a N_{\tau}} \|\rho(\epsilon, \alpha, d)\|_{\mathbf{P}}^2 = \frac{1}{2N_a N_{\tau}} \sum_{n=1}^2 \sum_{i=1}^{N_a} \sum_{j=1}^{N_{\tau}} P_{ij} \left(\widehat{D}_{\tau_j}^{(n)}(a_i) - D_{\tau_j}^{(n)}(a_i; \epsilon, \alpha, d) \right)^2, \quad (2.8)$$

where $\mathbf{P} \in \mathbb{R}^{2N_a N_{\tau} \times 2N_a N_{\tau}}$ is a diagonal matrix, with each entry representing the experimental probability density P_{ij} measured at $a = a_i$ and $\tau = \tau_j$, and $\rho(\epsilon, \alpha, d) \in \mathbb{R}^{2N_a N_{\tau}}$ is a residual vector whose entries are $\widehat{D}_{\tau_j}^{(n)}(a_i) - D_{\tau_j}^{(n)}(a_i; \epsilon, \alpha, d)$. Clearly, the core step in the computation of $E(\epsilon, \alpha, d)$ is an evaluation of the residual $\rho(\epsilon, \alpha, d)$. The evaluation procedure of $\rho(\epsilon, \alpha, d)$ using the equations (2.6) and (2.7) is summarized in Algorithm 1.

Algorithm 1 Evaluation of the residual $\rho(\epsilon, \alpha, d)$

INPUTS: parameters ϵ , α , and d , estimates of the finite-time Kramer–Moyal coefficients $\{\widehat{D}_{\tau_j}^{(n)}(a_i) : 1 \leq n \leq 2, 1 \leq i \leq N_a, 1 \leq j \leq N_\tau\}$

OUTPUTS: residual vector $\rho(\epsilon, \alpha, d)$

- Solve the adjoint Fokker–Planck equation (2.6). $(1 \leq n \leq 2, 1 \leq i \leq N_a, 1 \leq j \leq N_\tau)$
 - Compute $D_{\tau_j}^{(n)}(a_i)$ by invoking the formula (2.7). $(1 \leq n \leq 2, 1 \leq i \leq N_a, 1 \leq j \leq N_\tau)$
 - Compute each entry $\widehat{D}_{\tau_j}^{(n)}(a_i) - D_{\tau_j}^{(n)}(a_i; \epsilon, \alpha, d)$ of $\rho(\epsilon, \alpha, d)$. $(1 \leq n \leq 2, 1 \leq i \leq N_a, 1 \leq j \leq N_\tau)$
-

Finally, the optimization of the system coefficients is done by solving the following minimization problem:

$$\min_{\epsilon, \alpha, d} E(\epsilon, \alpha, d). \quad (2.9)$$

It was demonstrated mathematically in [41] that ℓ^2 -minimization models such as (2.9) are robust to additive measurement noise. In [22, 23], the Nelder–Mead algorithm [30] was adopted to solve (2.9). In the next section, on the contrary, we take a further step and propose a novel numerical algorithm for more efficiently solving (2.9).

3. Proposed algorithm

Although the Nelder–Mead algorithm has been successfully demonstrated for system identification of stochastic oscillators in [22, 23], it suffers from some well-known drawbacks. For example, the convergence rate of the Nelder–Mead algorithm is known to be fairly slow; it was shown in [42] that the convergence rate deteriorates as the dimension of the unknown increases in general. Moreover, the algorithm may converge to a nonstationary point even if the cost function enjoys good properties such as strict convexity and differentiability [43].

In this section, we propose a new derivative-free algorithm for solving the minimization problem (2.9) with better performance. To construct a tailored algorithm for (2.9), we first observe several particular properties of the minimization problem (2.9) and its cost function (2.8).

Property 1. The minimization problem (2.9) is a nonlinear least squares problem.

Clearly, (2.9) can be regarded as a weighted nonlinear least squares problem that has three model parameters ϵ , α , and d , and $2N_\tau N_a$ observations $\widehat{D}_{\tau_j}^{(n)}(a_i)$, $1 \leq n \leq 2, 1 \leq i \leq N_a, 1 \leq j \leq N_\tau$. Hence, various numerical solvers such as Gauss–Newton-type methods, gradient methods, and direct search methods can be considered; see, e.g., [35] for a survey on numerical solvers for nonlinear least squares problems. To decide which one is most suitable for solving (2.9), we investigate further properties of the cost function (2.8).

Property 2. The computational cost for an evaluation of the cost function $E(\epsilon, \alpha, d)$ is high.

As shown in Algorithm 1, one has to solve $2N_a N_\tau$ initial-boundary value problems of the form (2.6) numerically in a single evaluation of the residual $\rho(\epsilon, \alpha, d)$. It means that the computational cost for an evaluation of the cost function (2.8) is considerably high. Hence, for numerical efficiency, direct search methods such as the Nelder–Mead algorithm should be avoided since they require a huge number of evaluations of the cost function in general. Instead, Gauss–Newton type methods that require the information of the first-order derivatives may be considered.

At each iteration of a Gauss–Newton type method for solving (2.9), one has to solve a linear system (see (3.2)) regarding the Jacobian $\mathbf{J}(\epsilon, \alpha, d)$ of the residual $\rho(\epsilon, \alpha, d)$. Thanks to the following property of the minimization problem (2.9), the computational cost for solving such a linear system becomes marginal.

Property 3. The number of unknown parameters in (2.9) is much smaller than the number of observations for fitting.

Property 3 is straightforward since 3 is far less than $2N_a N_\tau$. The dimension of the Jacobian $\mathbf{J} = \mathbf{J}(\epsilon, \alpha, d)$ is $2N_a N_\tau \times 3$, so that the matrix $\mathbf{J}^T \mathbf{P} \mathbf{J}$ arising in the direction search equation has the size 3×3 . Hence, the linear system can be solved in a fairly short time even if the number of observations is very large. This observation suggests us to adopt a Gauss–Newton type method to solve (2.9). In particular, the Levenberg–Marquardt algorithm [34] is a good option since it is well-known to show the robust and fast convergence behavior compared to other Gauss–Newton type methods. However, the following property of the residual $\rho(\epsilon, \alpha, d)$ makes the situation not so straightforward.

Property 4. The Jacobian $\mathbf{J}(\epsilon, \alpha, d)$ of the residual $\rho(\epsilon, \alpha, d)$ has no closed-form formula.

Because the term $D_{\tau_j}^{(n)}(a_i; \epsilon, \alpha, d)$ in (2.8) relies on the solutions of initial-boundary problems of the form (2.6), neither a closed-form formula nor a computationally cheap algorithm is available for finding the Jacobian \mathbf{J} accurately. Hence, the vanilla Levenberg–Marquardt algorithm is not directly applicable to (2.9).

The proposed algorithm is a modification of the Levenberg–Marquardt algorithm for (2.9) so that it does not require the first-order derivatives of the cost function $E(\epsilon, \alpha, d)$. In the proposed algorithm, we consider replacing \mathbf{J} in the Levenberg–Marquardt algorithm by a finite difference approximation $\tilde{\mathbf{J}} = \tilde{\mathbf{J}}(\epsilon, \alpha, d)$:

$$\tilde{\mathbf{J}}(\epsilon, \alpha, d) = \begin{bmatrix} \frac{\rho(\epsilon + \Delta\epsilon, \alpha, d) - \rho(\epsilon, \alpha, d)}{\Delta\epsilon} & \frac{\rho(\epsilon, \alpha + \Delta\alpha, d) - \rho(\epsilon, \alpha, d)}{\Delta\alpha} & \frac{\rho(\epsilon, \alpha, d + \Delta d) - \rho(\epsilon, \alpha, d)}{\Delta d} \end{bmatrix}, \quad (3.1)$$

where $\Delta\epsilon$, $\Delta\alpha$, and Δd are nonzero real constants sufficiently near 0; we set

$$\Delta\epsilon = \max \left\{ \frac{|\epsilon|}{10}, 10^{-5} \right\}, \quad \Delta\alpha = \max \left\{ \frac{|\alpha|}{10}, 10^{-5} \right\}, \quad \Delta d = \max \left\{ \frac{|d|}{10}, 10^{-5} \right\}$$

heuristically. Note that a single evaluation of the approximate Jacobian $\tilde{\mathbf{J}}(\epsilon, \alpha, d)$ in (3.1) requires four evaluations of the residual: $\rho(\epsilon, \alpha, d)$, $\rho(\epsilon + \Delta\epsilon, \alpha, d)$, $\rho(\epsilon, \alpha + \Delta\alpha, d)$, and $\rho(\epsilon, \alpha, d + \Delta d)$.

Once the approximate Jacobian $\tilde{\mathbf{J}}$ has been obtained, the search direction $\Delta\theta$ is computed by solving the following linear system:

$$\left(\tilde{\mathbf{J}}^T \mathbf{P} \tilde{\mathbf{J}} + \lambda \text{diag} \left(\tilde{\mathbf{J}}^T \mathbf{P} \tilde{\mathbf{J}} \right) \right) \Delta\theta = \tilde{\mathbf{J}}^T \mathbf{P} \rho(\theta), \quad (3.2)$$

where $\theta = [\epsilon, \alpha, d]^T$ and λ is a positive damping factor adjusted at each iteration by the Marquardt rule [34]. An initial value λ_0 for the damping factor λ does not affect to the convergence behavior, and we simply set $\lambda_0 = 1$.

Algorithm 2 Proposed algorithm for solving (2.9)

INPUTS: system state $x(t)$, set of amplitudes $\{a_i\}_{i=1}^{N_a}$, set of time-shifts $\{\tau_j\}_{j=1}^{N_\tau}$

OUTPUTS: parameters ϵ , α , and d

• Compute $\tilde{D}_{\tau_j}^{(n)}(a_i)$ from $x(t)$ using (2.5). ($1 \leq n \leq 2, 1 \leq i \leq N_a, 1 \leq j \leq N_\tau$)

• Set the initial guess $(\epsilon^{(0)}, \alpha^{(0)}, d^{(0)})$ by the output of Algorithm 3.

for $k = 0, 1, 2, \dots$ **do**

• Compute the approximate Jacobian $\tilde{\mathbf{J}} = \tilde{\mathbf{J}}(\theta^{(k)})$ by invoking the formula (3.1).

• Solve the linear system (3.2) with $\lambda = \lambda_k$ to find a candidate $\Delta\theta_0$ for the search direction.

• Solve the linear system (3.2) with $\lambda = \lambda_k/2$ to find a candidate $\Delta\theta_{-1}$ for the search direction.

if $E(\theta^{(k)} - \Delta\theta_0) > E(\theta^{(k)})$ and $E(\theta^{(k)} - \Delta\theta_{-1}) > E(\theta^{(k)})$ **then**

• Find the smallest $m > 0$ such that $E(\theta^{(k)} - \Delta\theta_m) \leq E(\theta^{(k)})$, where $\Delta\theta_m$ is the solution of (3.2) with $\lambda = 2^m \lambda_k$.

• Set $\theta^{(k+1)} = \theta^{(k)} - \Delta\theta_m$ and $\lambda_{k+1} = 2^m \lambda_k$.

else

if $E(\theta^{(k)} - \Delta\theta_0) \leq E(\theta^{(k)} - \Delta\theta_{-1})$ **then**

• Set $\theta^{(k+1)} = \theta^{(k)} - \Delta\theta_0$ and $\lambda_{k+1} = \lambda_k$.

else

• Set $\theta^{(k+1)} = \theta^{(k)} - \Delta\theta_{-1}$ and $\lambda_{k+1} = \lambda_k/2$.

end if

end if

• Check the stop criteria.

end for

Finally, we summarize the proposed algorithm in Algorithm 2. It is well-known that Gauss–Newton type methods require a good initial guess for the unknown θ to ensure good performance [44]. In the proposed method, we obtain a reliable initial guess $\theta^{(0)}$ by the extrapolation method (see Algorithm 3). Note that the main computational cost of Algorithm 3 comes from two linear least-square problems (B.2) and (B.4), so it is minor compared to the computational cost of a single iteration of the proposed algorithm. Efficient implementation of Algorithm 2 on a multiprocessing computer system is discussed in Appendix C.

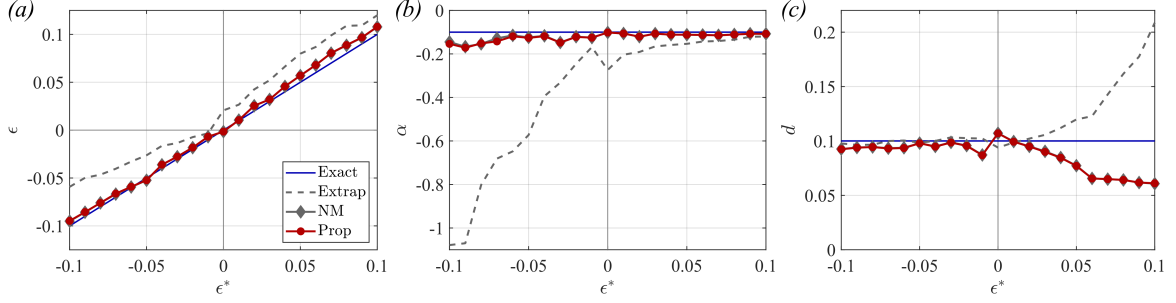


Figure 1: Numerical results of system identification using three different algorithms: Extrap (Algorithm 3), NM (Nelder–Mead algorithm), and Prop (Algorithm 2). Exact values for the parameters in the Van der Pol oscillator (2.1) are chosen as $-0.1 \leq \epsilon^* \leq 0.1$, $\alpha^* = -0.1$, $d^* = 0.1$, and $\omega^* = 2\pi$. All values presented in this figure are averaged over 50 independent trials with respect to random noise η in (2.1). Blue lines denote the true values of the input parameters ϵ , α , and d in (2.1).

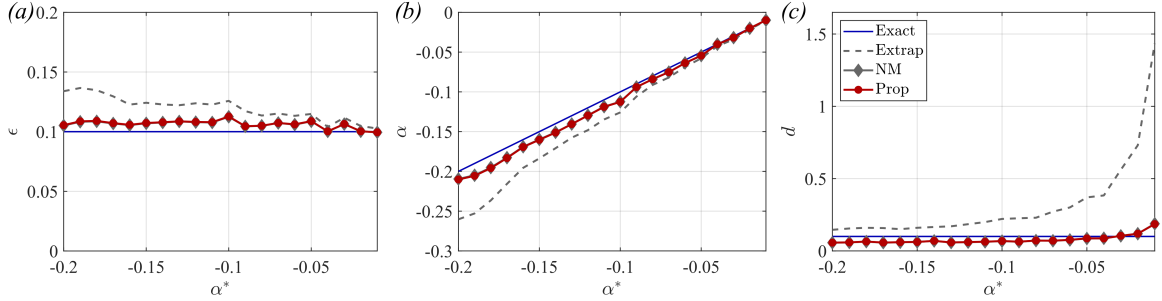


Figure 2: Numerical results of system identification using three different algorithms: Extrap (Algorithm 3), NM (Nelder–Mead algorithm), and Prop (Algorithm 2). Exact values for the parameters in the Van der Pol oscillator (2.1) are chosen as $\epsilon^* = 0.1$, $-0.2 \leq \alpha^* \leq -0.01$, and $d^* = 0.1$. All values presented in this figure are averaged over 50 independent trials with respect to random noise η in (2.1). Blue lines denote the true values of the input parameters ϵ , α , and d in (2.1).

4. Demonstration and validation of the system-identification framework

4.1. Synthetic data

In order to demonstrate the performance of the proposed algorithm, we first conduct numerical simulations on synthetic data. A numerical Van der Pol oscillator perturbed by Gaussian white noise is chosen as the target system, and the system identification is repeatedly performed with varying linear ($-0.1 \leq \epsilon \leq +0.1$) and nonlinear ($-0.2 \leq \alpha \leq -0.01$) coefficients, with an interval of 0.01 each. d , ω , N_a and N_τ are fixed at 0.1, 2π , 50 and 100, respectively. The set of amplitudes $\{a_i\}_{i=1}^{N_a}$ is chosen as the equipartitioning points of the range of $a(t)$. As for the time-delay input, we select τ_j so that the time-lagged signal has significant correlation with the original signal. That is, the set of time-delay values $\{\tau_j\}_{j=1}^{N_\tau}$ is selected from the equipartitioned interval $[\tau_1, \tau_2]$, where the lower bound τ_1 is the time lag that makes the autocorrelation of the signal drops below 0.97 for $\epsilon > 0$ and 0.6 for $\epsilon \leq 0$. The upper bound τ_2 is chosen to be 100 times the lower bound τ_1 .

In order to compensate the randomness of the experiments, each case is repeated 50 times with different random seeds while the results are averaged. We compare the results of extrapolation-based output-only system identification without optimization, existing output-only system identification combined with Nelder–Mead optimization [22], and the proposed system-identification framework introduced in Section 3. Stop criteria for the optimization are described below and are applied for both the Nelder–Mead algorithm and the proposed algorithm:

$$\frac{\|\theta^{(n+1)} - \theta^{(n)}\|_{\ell^2}}{1 + \|\theta^{(n)}\|_{\ell^2}} < 10^{-4} \quad \text{and} \quad \frac{|E(\theta^{(n+1)}) - E(\theta^{(n)})|}{1 + |E(\theta^{(n)})|} < 10^{-4}.$$

MATLAB pdepe program is used as a numerical solver for the adjoint Fokker–Planck equation (2.6), in which the spatial and time discretizations are done by the method proposed in [45] and the ode15s program described in [46],

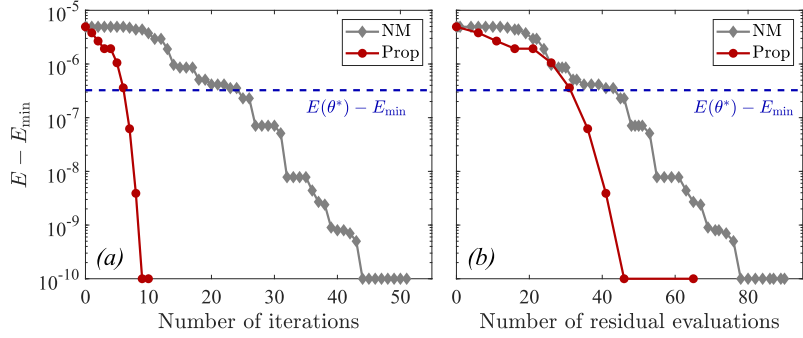


Figure 3: Decay of the energy error $E(\theta^{(n)}) - E_{\min}$ for the Nelder–Mead algorithm (NM) and Algorithm 2 (Prop) with respect to (a) the number of iterations and (b) the number of residual evaluations, where E_{\min} is the energy value at the converged point (both algorithms converge to the same point). The blue dashed line indicates $E(\theta^*) - E_{\min}$, where $\theta^* = (\epsilon^*, \alpha^*, d^*) = (0.1, -0.1, 0.1)$ denotes the exact values for the parameters.

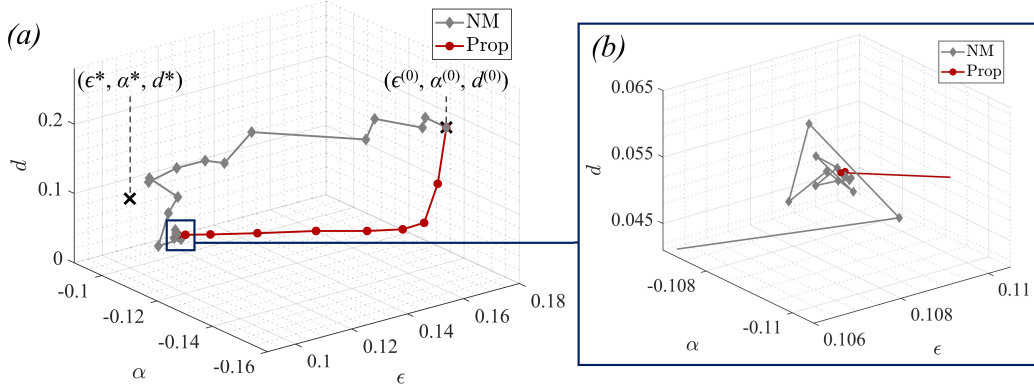


Figure 4: Trajectories of the sequences $\{(\epsilon^{(n)}, \alpha^{(n)}, d^{(n)})\}$ generated by two algorithms NM (Nelder–Mead algorithm) and Prop (Algorithm 2) plotted in the three-dimensional (ϵ, α, d) -space. The red point $(\epsilon^*, \alpha^*, d^*) = (0.1, -0.1, 0.1)$ indicates the exact values for the parameters, and the blue point $(\epsilon^{(0)}, \alpha^{(0)}, d^{(0)})$ indicates the initial guess obtained by Algorithm 3.

respectively. All codes are programmed using MATLAB R2021a and performed on a computer equipped with two Intel Xeon Gold 6240R CPUs (2.4GHz, 24C), 192GB RAM, and the operating system CentOS 7.8 64-bit.

Figures 1 and 2 show results of system identification performed to the systems with varying ϵ and α , respectively. When the linear coefficient ϵ is varied, it can be found from Figure 1(a) that the extrapolation-based system identification gives a reasonable result, especially when $|\epsilon^*|$ is small. However, identified nonlinear coefficient α and the noise amplitude d are found to be inaccurate when such a method is applied, specifically in the case where ϵ^* is either too small (Figure 1(b)) or too large (Figure 1(c)). One of the factors that cause this inaccuracy is the aforementioned finite-time effect arising from the small τ region. When this adverse effect is relieved with the optimization scheme, system-identification accuracy for ϵ , α , and d dramatically increase. Interestingly, the accuracy of the existing method that uses the Nelder–Mead algorithm and the proposed algorithm has minimal differences. That is, we conclude that both the Nelder–Mead and proposed algorithms solve the minimization problem (2.9) accurately and find the same local minimum. The advantage of the proposed algorithm, however, will soon become clear.

Similar trends are found when the nonlinear coefficient α is varied. In Figure 2, extrapolation-based system identification yields an understandable results for ϵ and α , but the error is greater for d with an exponential growth of identified d at large α region (see Figure 2(c)). From either the Nelder–Mead optimization or the proposed algorithm, accurate values of ϵ , α , and d are obtained.

We now inspect the computational efficiency of the proposed system-identification method. Figure 3 is the convergence plot showing the decay of the energy error $E(\theta^{(k)}) - E_{\min}$ with respect to the number of iterations k , where E_{\min} is the cost value at the converged point. It can be found that, although the existing method (Nelder–Mead based

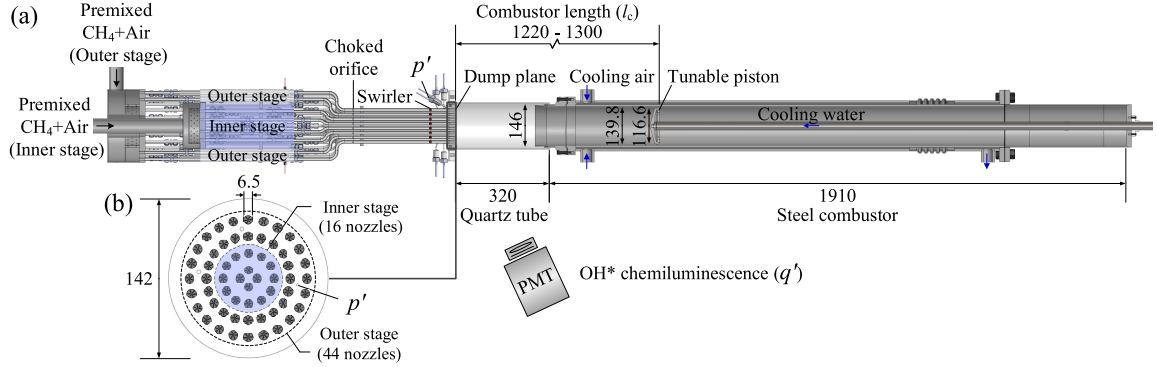


Figure 5: Experimental setup of a mesoscale multi-nozzle model gas-turbine combustor with variable length for acquiring data used in this study, of which the cross-sectional view is shown in (a). This setup constitutes sixty swirl injectors, whose spatial arrangement at the combustor dump plane is shown in (b). At the combustor dump plane, acoustic pressure fluctuation (p') of the combustor is measured with a piezoelectric transducer. All dimensions are in millimeters. This figure is identical to [47, Figure 1].

Segment No.	1	2	3	4	5	6	7	8	9	10	11	12	13	14
NM	332	279	300	258	310	295	319	281	291	220	231	275	268	253
Prop	21	21	16	19	18	16	16	131	118	71	63	78	74	74

Segment No.	15	16	17	18	19	20	21	22	23	24	25	26	27	28
NM	N/A	N/A	286	277	331	365	292	279	312	338	315	327	335	278
Prop	92	130	82	88	94	101	136	91	88	93	89	106	90	91

Table 1: Number of residual evaluations in the Nelder–Mead algorithm (NM) and the proposed method (Prop) for system identification with gas-turbine combustor data. N/A means that the method is not convergent. Each segment corresponds to a time-series data of 0.25 seconds.

optimization) and the proposed algorithm (Algorithm 2) reach a similar cost error, the latter requires a much lower number of iterations and residual evaluations. This means that the system identification can be performed much faster using the proposed algorithm, while its accuracy is maintained. The numerical efficiency of the proposed algorithm is further displayed in Figure 4. The convergence trajectory shows that the coefficients are seamlessly converged to the target value, showing that our tailored optimization scheme works excellently for the system identification.

4.2. Gas-turbine combustor data

To further validate the developed framework on a realistic physical system, we use the data obtained from a model gas-turbine data identical to [47]. This data features a transient development from the combustion noise to thermoacoustic instability of a combustor containing the methane-air premixed flame. A detailed description of the experimental setup used to acquire this data can be found in [47, 48]. In brief, this setup shown in Figure 5 enables the generation of thermoacoustic limit-cycle by adjusting the combustor length with the tunable piston. While varying the combustor length, pressure fluctuation p' , which is treated as a system variable x in equation (2.1), is measured with a piezoelectric transducer (PCB 112A22, 14.5 mV/kPa).

By using a motorized traverse with a constant speed, the tunable piston is swept from 1220 mm to 1300 mm. Meanwhile, pressure fluctuation data is obtained with a sampling rate of 12 kHz for 7 seconds. The time evolution of p' and its amplitude during the sweep are shown in Figure 6(b). The time-series signal indicates that the system transitions from the low-amplitude oscillation to the high-amplitude limit-cycle oscillation at $t \approx 2.5s$ ($l_c \approx 1250$). We slice this time-series data into 28 pieces (0.25 seconds per segment) and conduct output-only system identification for each one-second segment. System identification results displayed in Figure 6(c, d) show the trends of increasing ϵ , decreasing (and saturating) α upon the increase of combustor length l_c . We also find in Figure 6(e) that the amplitude of noise increases and saturates during the transition from stable fixed-point regime to the limit-cycle regime. These tendencies correctly capture the dynamics of the increasing fluctuation amplitude of the system variable p' .

To compare the computational efficiency of the Nelder–Mead and proposed algorithms, we present the number of residual evaluations in Table 1. We observe that the numbers of the proposed method are consistently much lower than

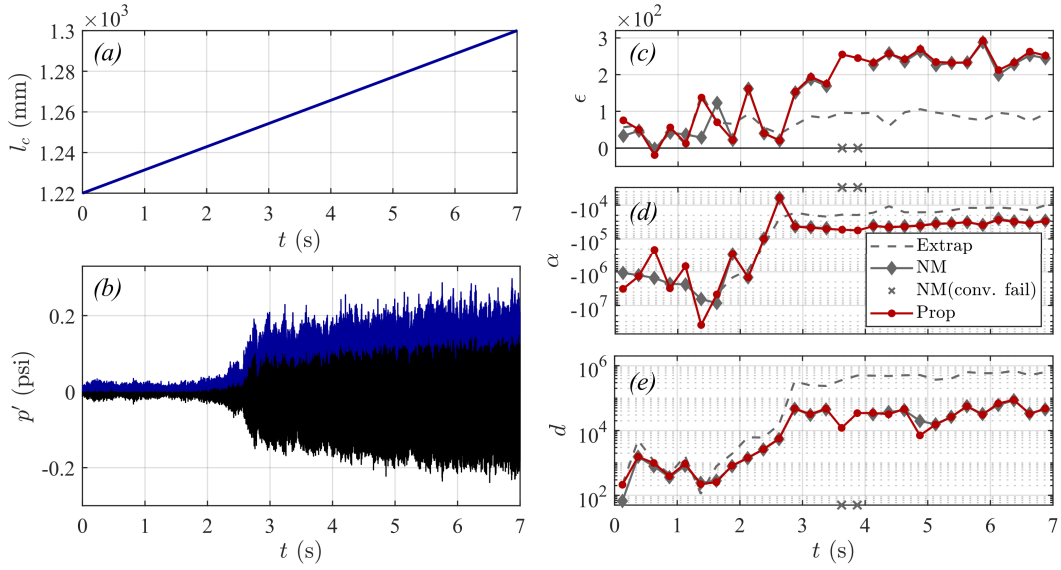


Figure 6: (a) Change in combustor length and the corresponding (b) time-series signal of the acoustic pressure fluctuation (black line) and its amplitude obtained from the Hilbert transform (blue line). (c) Linear (ϵ), (d) nonlinear (α) coefficients, and (e) noise amplitude (d) obtained from the output-only system identification based on extrapolation (gray dashed lines), Nelder–Mead algorithm (gray markers), and the proposed method (red markers). Cross markers indicate the convergence failure for Nelder–Mead optimization.

those of the Nelder–Mead algorithm. These results verify that the proposed method outperforms the Nelder–Mead algorithm in terms of computational efficiency for system identification, even when dealing with realistic data.

Notably, we find that the proposed method can compute the system parameters at $t = 3.5\text{--}3.75$ s, where the convergence of the Nelder–Mead algorithm has failed and the parameters could not be extracted. This is due to the poor optimization of the Nelder–Mead trajectory (cf. Figure 4), which causes it to fall into a regime where the underlying adjoint Fokker–Planck equation (2.6) becomes extremely stiff, leading to the failure of the numerical solver pdepe. In contrast, the proposed algorithm successfully avoids this regime and produces reliable results.

Finally, we compare the scales of deterministic and random parts of the noise-perturbed Van der Pol equation (see (2.1)). We computed the absolute value of the deterministic part (LHS) and the scale of stochasticity ($\sqrt{2d}$) using the system parameters obtained from the proposed method. The results displayed in Figure 7(a) shows that, while both the deterministic and stochastic parts strengthen while the combustor length increases, the ratio between these two parts tends to decrease. This means that the system becomes more deterministic as the system approaches and enters the thermoacoustic limit cycle. During such a process, the ratio between |LHS| and $\sqrt{2d}$ varies between 4200 and 550. This means that the noise acting on the system, regardless of its source, exerts 0.024–0.181% of randomness to the deterministic second-derivative dynamics of the combustor. This amount of stochasticity is converted into 33–46% deviation of the amplitude fluctuation in the stable fixed-point regime (0–1 s in the experiment; see Figure 7(b, c)), and 11–14% deviation in the fully developed limit-cycle regime (5–7 s in the experiment). Thus, We can conclude that the proposed method can be successfully applied to the data affected by intense noise—including the inherent, external, and measurement noises—which perturbs the original deterministic signal for a maximum of 46%.

5. Conclusion

In this paper, we proposed a numerically efficient system-identification framework for a stochastically driven self-sustained oscillator. In this framework, initial system parameters are extracted from the time-series data characterized by the Langevin equation and the corresponding Fokker–Planck equation. We then constructed an optimization model that extracts coefficients using the adjoint Fokker–Planck equation. We proposed a tailored algorithm for the optimization model, which is a derivative-free modification of the Levenberg–Marquardt algorithm. Computational aspects of the proposed algorithm are considered to enhance the computation speed on a parallel computer. We demonstrated the

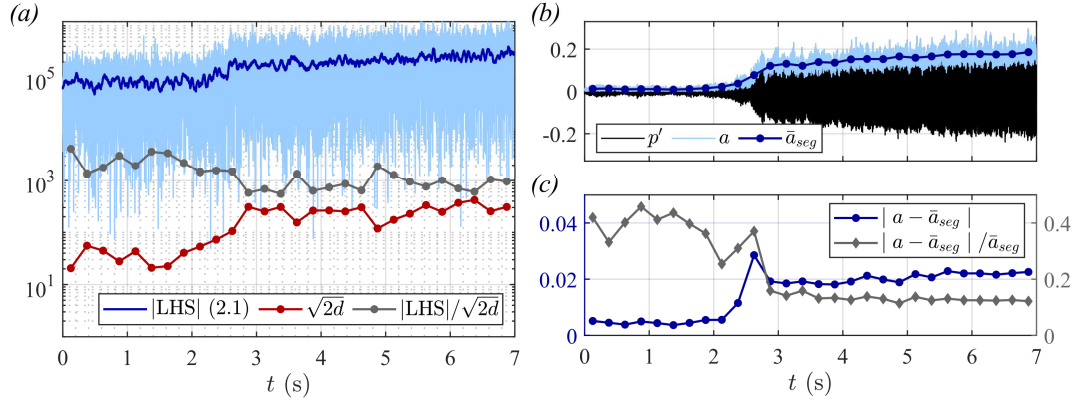


Figure 7: (a) A comparison between scales of the left- and right-hand side of equation 2.1. The light blue line indicates the absolute value of the left-hand side (LHS) of (2.1) computed with obtained coefficient, and the blue line is its average. The red line is the right-hand side of the same equation before the multiplication of Gaussian white noise. The grey line is the ratio between these two values. Y-axis is in the logarithmic scale. (b) The pressure fluctuation amplitude (light blue line) and its average in each data segment (blue points). (c) Deviation of pressure fluctuation amplitude due to the stochastic effects (blue points) and its ratio to the mean fluctuation amplitude in each segment (grey points).

proposed framework on both the numerical and experimental systems in the linearly stable state ($\epsilon < 0$) and linearly unstable state ($\epsilon > 0$) at self-sustained oscillation. As a result, we showed that the computational cost for identifying the system coefficients is greatly reduced without sacrificing the system-identification accuracy. From the analysis on stochasticity of the experimental data used in this study, we found that the proposed method can be applied to a highly noisy system.

A significant implication of this study is that the overall time required for performing the output-only system identification is substantially reduced. Considering that system identification is often required for the real-time monitoring and control of dynamical systems, the proposed framework opens up new possibilities for the instantaneous diagnosis and the feedback control of practical engineered systems.

As for the limitation of this study, the proposed framework is only applicable to the system where the amplitude and phase of the oscillation change slowly. In other words, the absolute value of the growth rate of the system should be sufficiently low. A representative case where such a condition is met is found near a Hopf bifurcation. This implies that the proposed system-identification framework can nevertheless be used to diagnose or predict the instability features near a supercritical or subcritical Hopf bifurcation [37].

CRediT authorship contribution statement

Minwoo Lee: Conceptualization, Validation, Investigation, Visualization, Writing. **Kyu Tae Kim:** Validation, Investigation, Data curation. **Jongho Park:** Methodology, Software, Investigation, Resources, Writing.

Declaration of competing interest

The authors declare that they have no known competing financial interests or personal relationships that could have appeared to influence the work reported in this paper.

Acknowledgement

Minwoo Lee was supported by the National Research Foundation of Korea (NRF) grant funded by the Korean government (MSIT) (No. 2021R1G1A1091278). Kyu Tae Kim was supported by NRF grant funded by MSIT (No. 2022R1A2B5B01001554). Jongho Park's work was supported by NRF grant funded by MSIT (No. 2021R1C1C2095193).

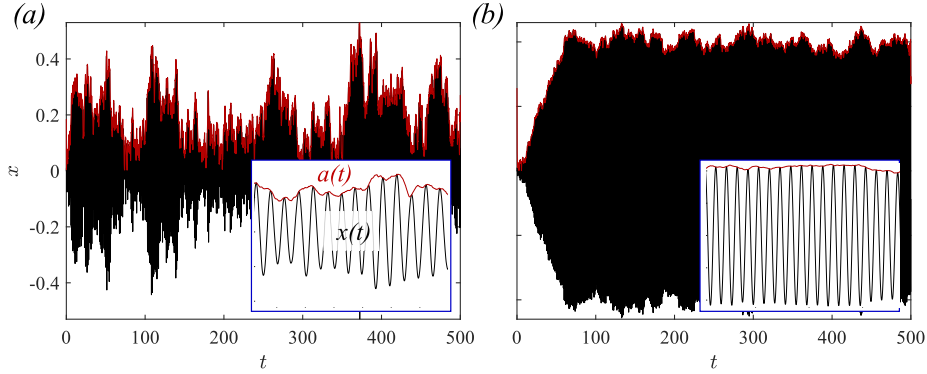


Figure A.8: The system state $x(t)$ and amplitude $a(t)$ of stochastically forced oscillators in **(a)** linearly stable state $(\epsilon, \alpha) = (-0.1, -0.1)$ and **(b)** linearly unstable state $(\epsilon, \alpha) = (0.1, -0.1)$. ω and d are set to 2π and 0.1 , respectively. The amplitude $a(t)$ is obtained from the Hilbert transform of $x(t)$. In both cases, $a(t)$ varies much slower than $x(t)$ (cf. [7, Figure 3]).

Appendix A. Derivation of the Fokker–Planck equation (2.2)

In this appendix, we provide a detailed derivation of the Fokker–Planck equation (2.2) from the Langevin equation (2.1). We first apply the method of variation of parameters [49] in (2.1). In other words, we transform the instantaneous state of the system $x(t)$ into its amplitude $a(t)$ and phase $\phi(t)$ as follows [50, 51]:

$$x = a(t) \cos(\omega t + \phi(t)),$$

$$\frac{dx}{dt} = -a(t)\omega \sin(\omega t + \phi(t)).$$

An illustration of the signal $x(t)$ and the amplitude $a(t)$ is shown in Figure A.8. From the substitution of variables and applying trigonometric identities, we obtain a system of ordinary differential equations with respect to $a(t)$ and $\phi(t)$ as follows [7]:

$$\frac{da}{dt} = \frac{\epsilon}{2}a + \frac{\alpha}{8}a^3 + Q_1(\Phi) - \left(\frac{\sqrt{2d}}{\omega} \sin \Phi\right) \eta, \quad (\text{A.1a})$$

$$\frac{d\phi}{dt} = Q_2(\Phi) - \left(\frac{\sqrt{2d}}{\omega a} \cos \Phi\right) \eta, \quad (\text{A.1b})$$

where $\Phi(t) = \omega t + \phi(t)$, and $Q_1(\Phi)$ and $Q_2(\Phi)$ are the sum of all the terms with first-order cosine components appearing in (A.1a) and (A.1b), respectively. By assuming that $a(t)$ and $\Phi(t)$ are slow variables (see Figure A.8), $Q_1(\Phi)$ and $Q_2(\Phi)$ become zero upon time averaging. It is worth mentioning that, in the noise-free case ($d = 0$), (A.1a) reduces to the normal-form equation of Hopf bifurcation:

$$\frac{da}{dt} = \frac{\epsilon}{2}a + \frac{\alpha}{8}a^3.$$

For nonzero case, on the contrary, stochastic averaging [52, 53] can be applied to (A.1), yielding the following Fokker–Planck equation (2.2) whose unknown is the transitional probability density function $P(a, t)$ of a at time t :

$$\frac{\partial}{\partial t} P(a, t) = -\frac{\partial}{\partial a} [D^{(1)}(a)P(a, t)] + \frac{\partial^2}{\partial a^2} [D^{(2)}(a)P(a, t)], \quad a > 0, t > 0,$$

$$P(a, 0) = P_0(a), \quad a > 0,$$

$$P(0, t) = 0, \quad t > 0.$$

Note that the Kramer–Moyal coefficients $D^{(1)}(a)$ and $D^{(2)}(a)$ were given in (2.3).

Appendix B. Extrapolation method for system identification

In this appendix, we present the extrapolation method for system identification of a self-sustained oscillator under stochastic forcing modeled by the Langevin equation (2.1). Likewise the optimization method described in Section 2, we estimate the Kramer–Moyal coefficients $D^{(1)}(a)$ and $D^{(2)}(a)$ in (2.2). We assume that the amplitude and time spaces are discretized as in Section 2. Namely, we have a set of amplitudes $\{a_i\}_{i=1}^{N_a}$ and a set of time-shifts $\{\tau_j\}_{j=1}^{N_\tau}$. Recall that the estimate $\widehat{D}_{\tau_j}^{(n)}(a_i)$ ($n = 1, 2$) for $D_{\tau_j}^{(n)}(a_i)$ is computed by (2.5). In order to estimate $D^{(n)}(a)$ at zero time-delay limit (2.4), one may consider extrapolating finite-time drift and diffusion terms toward $\tau = 0$, as depicted in Figure B.9. Specifically, we extrapolate $\widehat{D}_{\tau_j}^{(n)}(a_i)$ using an exponential fit [23]. For fixed n and a_i , we assume that

$$\widehat{D}_{\tau_j}^{(n)}(a_i) \approx \exp\left(c_1^{(n)}(a_i)\tau_j + c_0^{(n)}(a_i)\right)$$

for some constants $c_0^{(n)}(a_i)$ and $c_1^{(n)}(a_i)$. Equivalently, we have

$$\log \widehat{D}_{\tau_j}^{(n)}(a_i) \approx c_1^{(n)}(a_i)\tau_j + c_0^{(n)}(a_i). \quad (\text{B.1})$$

The least-squares solution of (B.1) with respect to $\tau = \tau_1, \dots, \tau_{N_\tau}$ is given by

$$\begin{bmatrix} c_0^{(n)}(a_i) \\ c_1^{(n)}(a_i) \end{bmatrix} = (\mathbf{A}^T \mathbf{A})^{-1} \mathbf{A} \mathbf{b}, \quad (\text{B.2a})$$

where

$$\mathbf{A} = \begin{bmatrix} 1 & \tau_1 \\ \vdots & \vdots \\ 1 & \tau_{N_\tau} \end{bmatrix}, \quad \mathbf{b} = \begin{bmatrix} \log \widehat{D}_{\tau_1}^{(n)}(a_i) \\ \vdots \\ \log \widehat{D}_{\tau_{N_\tau}}^{(n)}(a_i) \end{bmatrix}. \quad (\text{B.2b})$$

Note that $\mathbf{A}^T \mathbf{A}$ is invertible whenever all τ_j 's are distinct. The τ -extrapolation of the diffusion term $\widehat{D}_\tau^{(2)}(a_i)$ toward $\tau = 0$ yields

$$d = 2\omega^2 D^{(2)}(a_i) = 2\omega^2 \lim_{\tau \rightarrow 0} D_\tau^{(2)}(a_i) \approx 2\omega^2 \exp\left(c_0^{(2)}(a_i)\right),$$

so that we may approximate d by

$$d \approx \frac{2\omega^2}{N_a} \sum_{i=1}^{N_a} \exp\left(c_0^{(2)}(a_i)\right). \quad (\text{B.3})$$

Similarly, from the τ -extrapolation of the drift term $\widehat{D}_\tau^{(1)}(a_i)$, we have

$$\frac{\epsilon}{2}a_i + \frac{\alpha}{8}a_i^3 + \frac{d}{2\omega^2 a_i} = D^{(1)}(a_i) = \lim_{\tau \rightarrow 0} D_\tau^{(1)}(a_i) \approx \exp\left(c_0^{(1)}(a_i)\right).$$

In order to identify ϵ and α from the above relation, we solve the following least-squares problem with respect to $a = a_1, \dots, a_{N_a}$:

$$\begin{bmatrix} \epsilon \\ \alpha \end{bmatrix} = (\widetilde{\mathbf{A}}^T \widetilde{\mathbf{A}})^{-1} \widetilde{\mathbf{A}} \widetilde{\mathbf{b}}, \quad (\text{B.4a})$$

where

$$\widetilde{\mathbf{A}} = \begin{bmatrix} \frac{a_1}{2} & \frac{a_1^3}{8} \\ \vdots & \vdots \\ \frac{a_{N_a}}{2} & \frac{a_{N_a}^3}{8} \end{bmatrix}, \quad \widetilde{\mathbf{b}} = \begin{bmatrix} \exp\left(c_0^{(1)}(a_1)\right) - \frac{d}{2\omega^2 a_1} \\ \vdots \\ \exp\left(c_0^{(1)}(a_{N_a})\right) - \frac{d}{2\omega^2 a_{N_a}} \end{bmatrix}. \quad (\text{B.4b})$$

In (B.4), the matrix $\widetilde{\mathbf{A}}^T \widetilde{\mathbf{A}}$ is invertible if and only if all a_i 's are distinct. We summarize the overall procedure to find the parameters ϵ , α , and d by extrapolation in Algorithm 3.

Algorithm 3 Extrapolation process for finding $D^{(n)}$

INPUTS: system state $x(t)$, set of amplitudes $\{a_i\}_{i=1}^{N_a}$, set of time-shifts $\{\tau_j\}_{j=1}^{N_\tau}$

OUTPUTS: parameters ϵ , α , and d

- Compute $\widehat{D}_{\tau_j}^{(n)}(a_i)$ from $x(t)$ by invoking the formula (2.5). $(1 \leq n \leq 2, 1 \leq i \leq N_a, 1 \leq j \leq N_\tau)$
 - Compute $c_0^{(n)}(a_i)$ and $c_1^{(n)}(a_i)$ by solving the least-squares problem (B.2) with $a = a_i$. $(1 \leq n \leq 2, 1 \leq i \leq N_a)$
 - Compute d by invoking the formula (B.3).
 - Compute ϵ and α by solving the least-squares problem (B.4).
-

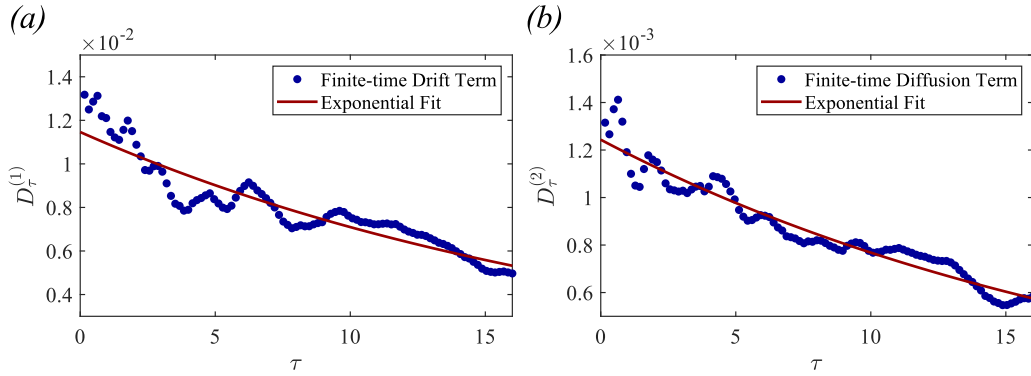


Figure B.9: Experimental (a) Drift and (b) diffusion terms obtained from (2.5) and the corresponding extrapolation toward $\tau = 0$ based on exponential fit (B.1). The results are obtained at $\epsilon = 0.1$, $\alpha = -0.1$, $d = 0.1$, $\omega = 2\pi$, and $a = 1.86$.

Figure B.9 shows numerically generated $D_\tau^{(n)}(a)$ at $a = 1.86$ and their regression $\widehat{D}_{\tau_j}^{(n)}(a_i)$ based on (B.1). Although the regression and the corresponding extrapolation reasonably represents the experimental $D_\tau^{(n)}(a)$, there exist some gap between $D_\tau^{(n)}(a)$ and $\widehat{D}_{\tau_j}^{(n)}(a_i)$, especially at small τ . This is because the finite-time effect that occurs due to the non-Markovian properties of the noise acting on the system comes into play. The finite-time effect becomes highly significant in the coarsely sampled data or the bandpass-filtered signal [22]. Because of this effect, the extrapolation-based drift and diffusion terms and the system parameters obtained from them contain an inherent inaccuracy. Nevertheless, it can be found from Figure B.9 that the exponential regression can reasonably reproduce the behavior of $D_\tau^{(n)}(a)$. Therefore, the system parameters obtained here can serve as a reliable initial guess for the proposed optimization-based system identification process proposed in this paper.

Appendix C. Implementation issues of the proposed algorithm

The appendix addresses computational efficiency and implementation considerations for the proposed algorithm. The computational efficiency of the algorithm is notably influenced by the total count of residual evaluations, as outlined in Property 2. We examine the number of residual evaluations needed during each iteration of Algorithm 2 and explore efficient strategies for implementing the algorithm on a multiprocessing computer system.

At the k th iteration of Algorithm 2, we require at least six values of the residual: at the points $\theta^{(k)}$, $\theta^{(k)} + (\Delta\epsilon, 0, 0)$, $\theta^{(k)} + (0, \Delta\alpha, 0)$, $\theta^{(k)} + (0, 0, \Delta d)$, $\theta^{(k)} - \Delta\theta_0$, and $\theta^{(k)} - \Delta\theta_{-1}$. Among them, $\rho(\theta^{(k)})$ need not to be evaluated because it has been already evaluated at the previous iteration and we are able to reuse it. Three values $\theta^{(k)} + (\Delta\epsilon, 0, 0)$, $\theta^{(k)} + (0, \Delta\alpha, 0)$, and $\theta^{(k)} + (0, 0, \Delta d)$ can be computed independently, hence they can be processed in parallel. Similarly, $\theta^{(k)} - \Delta\theta_0$ and $\theta^{(k)} - \Delta\theta_{-1}$ can be evaluated in parallel. Therefore, it requires approximately twice the residual evaluation time to evaluate the above-mentioned six residual values if parallel processing is efficiently utilized.

When both $E(\theta^{(k)} - \Delta\theta_0)$ and $E(\theta^{(k)} - \Delta\theta_{-1})$ are greater than $E(\theta^{(k)})$, we require m additional evaluations of the residual at the points $\theta^{(k)} - \Delta\theta_1, \dots, \theta^{(k)} - \Delta\theta_m$. Fortunately, it can be observed numerically that such a case seldom occurs and does not severely deteriorate the performance of the algorithm. Indeed, the Levenberg–Marquardt algo-

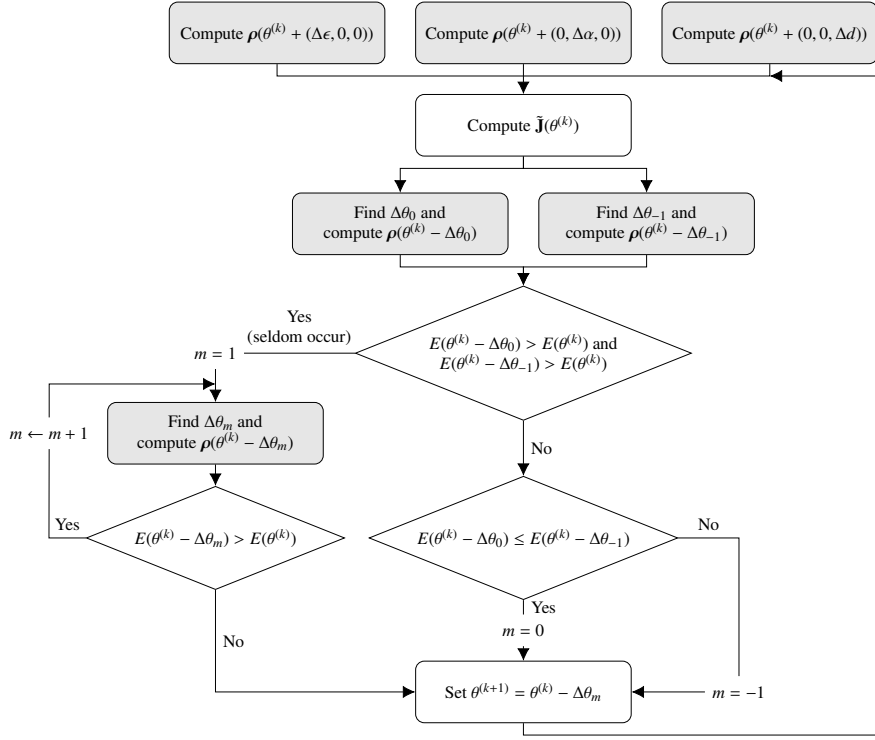


Figure C.10: Flow chart describing parallel implementation for the k th iteration of Algorithm 2. Items positioned in the same row can be processed in parallel. Items corresponding to residual evaluations are depicted in gray.

rithm is known to act more like the Gauss–Newton method, i.e., the damping factor λ decreases and the term $\tilde{\mathbf{J}}^T \mathbf{P} \tilde{\mathbf{J}}$ becomes more effective when the estimate $\theta^{(k)}$ becomes close to a local minimum of the cost function [54].

A flow chart for a single iteration of the proposed algorithm emphasizing the aspect of parallel computation is presented in Figure C.10. In Figure C.10, items positioned in the same row are independent to each other, so that they can be processed simultaneously on a parallel computer.

References

- [1] A. Pikovsky, M. Rosenblum, J. Kurths, Synchronization: A Universal Concept in Nonlinear Sciences, volume 12, Cambridge University Press, Cambridge, 2001.
- [2] H. Son, M. Lee, Continuous probabilistic solution to the transient self-oscillation under stochastic forcing: a PINN approach, *J. Mech. Sci. Technol.* 37 (2023) 3911–3918.
- [3] A. Balanov, N. Janson, D. Postnov, O. Sosnovtseva, Synchronization: From Simple to Complex, Springer, Berlin, 2008.
- [4] A. Jenkins, Self-oscillation, *Phys. Rep.* 525 (2013) 167–222.
- [5] J. Fuller, Heartbeat stars, tidally excited oscillations and resonance locking, *Mon. Notices Royal Astron. Soc.* 472 (2017) 1538–1564.
- [6] Y. Zhu, V. Gupta, L. K. B. Li, Onset of global instability in low-density jets, *J. Fluid Mech.* 828 (2017) R1.
- [7] M. Lee, Y. Zhu, L. K. B. Li, V. Gupta, System identification of a low-density jet via its noise-induced dynamics, *J. Fluid Mech.* 862 (2019) 200–215.
- [8] Y. Guan, V. Gupta, K. Kashinath, L. K. B. Li, Open-loop control of periodic thermoacoustic oscillations: experiments and low-order modelling in a synchronization framework, *P. Combust. Inst.* 37 (2019) 5315–5323.
- [9] M. Lee, Y. Guan, V. Gupta, L. K. B. Li, Input-output system identification of a thermoacoustic oscillator near a Hopf bifurcation using only fixed-point data, *Phys. Rev. E* 101 (2020) 013102.
- [10] E. Boujo, C. Bourquard, Y. Xiong, N. Noiray, Processing time-series of randomly forced self-oscillators: the example of beer bottle whistling, *J. Sound Vib.* 464 (2020) 114981.
- [11] T. Lieuwen, V. Yang, Combustion instabilities in gas turbine engines: operational experience, fundamental mechanisms and modeling, AIAA, Reston, 2005.
- [12] E. Negrini, G. Citti, L. Capogna, System identification through Lipschitz regularized deep neural networks, *J. Comput. Phys.* 444 (2021) 110549.

- [13] G. Karch, W. Wedig, Determination of Lyapunov exponents by weak solutions of Fokker–Planck equations, *Probabilistic Eng. Mech.* 10 (1995) 135–141.
- [14] M. Breccolotti, A. Materazzi, Identification of a non-linear spring through the Fokker–Planck equation, *Probabilistic Eng. Mech.* 23 (2008) 146–153.
- [15] Y. Liu, J. Sheng, R. Ding, Convergence of stochastic gradient estimation algorithm for multivariable ARX-like systems, *Comput. Math. Appl.* 59 (2010) 2615–2627.
- [16] W. Polifke, Black-box system identification for reduced order model construction, *Ann. Nucl. Energy* 67 (2014) 109–128.
- [17] C. Svardi, S. Jaensch, W. Polifke, Concurrent identification of aero-acoustic scattering and noise sources at a flow duct singularity in low Mach number flow, *J. Sound Vib.* 377 (2016) 90–105.
- [18] A. S. Pikovsky, J. Kurths, Coherence resonance in a noise-driven excitable system, *Phys. Rev. Lett.* 78 (1997) 775–778.
- [19] O. V. Ushakov, H. J. Wünsche, F. Henneberger, I. A. Khovanov, L. Schimansky-Geier, M. A. Zaks, Coherence resonance near a Hopf bifurcation, *Phys. Rev. Lett.* 95 (2005) 123903.
- [20] D. Yu, U. Parlitz, Estimating parameters by aut synchronization with dynamics restrictions, *Phys. Rev. E* 77 (2008) 066221.
- [21] N. Noiray, B. Schuermans, Deterministic quantities characterizing noise driven Hopf bifurcations in gas turbine combustors, *Int. J. Nonlin. Mech.* 50 (2013) 152 – 163.
- [22] E. Boujo, N. Noiray, Robust identification of harmonic oscillator parameters using the adjoint Fokker–Planck equation, *Proc. R. Soc. A* 473 (2017) 20160894.
- [23] M. Lee, K. T. Kim, V. Gupta, L. K. Li, System identification and early warning detection of thermoacoustic oscillations in a turbulent combustor using its noise-induced dynamics, *Proc. Combust. Inst.* 38 (2021) 6025–6033.
- [24] S. Nagarajaiah, B. Basu, Output only modal identification and structural damage detection using time frequency & wavelet techniques, *Earthq. Eng. Vib.* 8 (2009) 583–605.
- [25] S. Rudy, A. Alla, S. L. Brunton, J. N. Kutz, Data-driven identification of parametric partial differential equations, *SIAM J. Appl. Dyn. Syst.* 18 (2019) 643–660.
- [26] G. Bonciolini, E. Boujo, N. Noiray, Output-only parameter identification of a colored-noise-driven Van-der-Pol oscillator: thermoacoustic instabilities as an example, *Phys. Rev. E* 95 (2017) 062217.
- [27] M. Lee, D. Kim, J. Lee, Y. Kim, M. Yi, A data-driven approach for analyzing hall thruster discharge instability leading to plasma blowoff, *Acta Astronaut.* 206 (2023) 1–8.
- [28] S. J. Lade, Finite sampling interval effects in Kramers–Moyal analysis, *Phys. Lett. A* 373 (2009) 3705–3709.
- [29] C. Honisch, R. Friedrich, Estimation of Kramers–Moyal coefficients at low sampling rates, *Phys. Rev. E* 83 (2011) 066701.
- [30] J. C. Lagarias, J. A. Reeds, M. H. Wright, P. E. Wright, Convergence properties of the Nelder–Mead simplex method in low dimensions, *SIAM J. Optim.* 9 (1998) 112–147.
- [31] J. C. Lagarias, B. Poonen, M. H. Wright, Convergence of the restricted Nelder–Mead algorithm in two dimensions, *SIAM J. Optim.* 22 (2012) 501–532.
- [32] J. Berg, K. Nyström, Data-driven discovery of PDEs in complex datasets, *J. Comput. Phys.* 384 (2019) 239–252.
- [33] R. M. Lewis, V. Torczon, M. W. Trosset, Direct search methods: then and now, *J. Comput. Appl. Math.* 124 (2000) 191–207.
- [34] D. W. Marquardt, An algorithm for least-squares estimation of nonlinear parameters, *J. Soc. Ind. Appl. Math.* 11 (1963) 431–441.
- [35] Y.-X. Yuan, Recent advances in numerical methods for nonlinear equations and nonlinear least squares, *Numerical Algebra, Control & Optimization* 1 (2011) 15.
- [36] M. Lee, Numerical aspects of noise-induced dynamics in continuous combustion systems, *J. Korean Soc. Combust.* 28 (2023) 66–77.
- [37] M. Lee, System identification near a Hopf bifurcation via the noise-induced dynamics in the fixed-point regime, Ph.D. thesis, The Hong Kong University of Science and Technology, 2020.
- [38] A. Zakharova, T. Vadivasova, V. Anishchenko, A. Koseska, J. Kurths, Stochastic bifurcations and coherence-like resonance in a self-sustained bistable noisy oscillator, *Phys. Rev. E* 81 (2010) 011106.
- [39] S. Siegert, R. Friedrich, J. Peinke, Analysis of data sets of stochastic systems, *Phys. Lett. A* 243 (1998) 275–280. doi:10.1016/S0375-9601(98)00283-7.
- [40] M. Di Paola, A. Sofi, Approximate solution of the Fokker–Planck–Kolmogorov equation, *Probabilistic Eng. Mech.* 17 (2002) 369–384.
- [41] M. Lee, J. Park, An optimized dynamic mode decomposition model robust to multiplicative noise, *SIAM J. Appl. Dyn. Syst.* 22 (2023) 235–268.
- [42] L. Han, M. Neumann, Effect of dimensionality on the Nelder–Mead simplex method, *Optim. Methods Softw.* 21 (2006) 1–16.
- [43] K. I. M. McKinnon, Convergence of the Nelder–Mead simplex method to a nonstationary point, *SIAM J. Optim.* 9 (1998) 148–158.
- [44] T. Askham, J. N. Kutz, Variable projection methods for an optimized dynamic mode decomposition, *SIAM J. Appl. Dyn. Syst.* 17 (2018) 380–416.
- [45] R. D. Skeel, M. Berzins, A method for the spatial discretization of parabolic equations in one space variable, *SIAM J. Sci. Stat. Comput.* 11 (1990) 1–32.
- [46] L. F. Shampine, M. W. Reichelt, The MATLAB ODE suite, *SIAM J. Sci. Comput.* 18 (1997) 1–22.
- [47] M. Lee, Early warning detection of thermoacoustic instability using three-dimensional complexity-entropy causality space, *Exp. Therm. Fluid Sci.* 130 (2022) 110517.
- [48] H. Kang, T. Lee, U. Jin, K. T. Kim, Experimental investigation of combustion instabilities of a mesoscale multinozzle array in a lean-premixed combustor, *P. Combust. Inst.* 38 (2021) 6035 – 6042.
- [49] A. H. Nayfeh, Introduction to perturbation techniques, John Wiley, New York (1981).
- [50] J. Roberts, Stochastic averaging: An approximate method of solving random vibration problems, *Int. J. Non Linear Mech.* 21 (1986) 111–134.
- [51] W. Zhu, J. Yu, On the response of the Van der Pol oscillator to white noise excitation, *J. Sound Vib.* 117 (1987) 421 – 431.
- [52] R. L. Stratonovich, Topics in the Theory of Random Noise, Gordon and Breach, Philadelphia, 1963.
- [53] R. L. Stratonovich, Topics in the Theory of Random Noise: General theory of random processes; Nonlinear transformations of signals and

noise, Gordon and Breach, Philadelphia, 1967.

- [54] H. P. Gavin, The Levenberg–Marquardt algorithm for nonlinear least squares curve-fitting problems, 2019. URL: <https://people.duke.edu/~hpgavin/ce281/lm.pdf>, Department of Civil and Environmental Engineering, Duke University.